Analysis of CMOS Active Pixel Sensors as Linear Shift-Invariant Receivers

Jimmy C. Chau
Electrical and Computer Engineering
Boston University
Boston, Massachusetts 02215
Email: jchau@bu.edu

Thomas D.C. Little
Electrical and Computer Engineering
Boston University
Boston, Massachusetts 02215
Email: tdcl@bu.edu

***Abstract*—Although CMOS active pixel sensor (APS) cameras are used as receivers for low-bandwidth visible light communications (VLC), they have typically not been used to receive high-bandwidth VLC signals. However, by selectively scanning pixels on the image sensor, the sampling rate of CMOS APS pixels can be greatly improved, enabling them to capture high-bandwidth signals while maintaining the ability to scale to high image resolutions. To analyze CMOS APS image sensors for potential use in high data-rate applications, the CMOS active pixel is modeled as a linear shift-invariant (LSI) system. Using this LSI model, the frequency response (as a function of device and timing parameters) and the optimal exposure time for each sample are derived. The LSI model is also used to investigate the effects of clock-jitter on CMOS APS VLC receivers.**

I. Introduction

CMOS active pixel sensors (APS) are used in many ways for visible light communication (VLC). As the image sensor used in most smartphone cameras, CMOS APS image sensors are often used to capture 2D codes [1], [2] and their rolling shutters are often exploited to receive low data-rate VLC signals [3], [4]. CMOS APS image sensors are also used within high-speed cameras that track or receive VLC signals for vehicle-to-vehicle or vehicle-to-infrastructure communications [5]–[8].

Despite their many uses in VLC, to the best of the authors' knowledge, the impulse and frequency response of CMOS active pixels have not been previously investigated. This omission is likely because CMOS APS VLC receivers are most commonly used to capture low-bandwidth (less than 1 MHz) signals due to their relatively low frame rates. Instead, faster photodetectors based on transimpedance amplifiers (TIAs) are generally used to capture high-bandwidth VLC signals.

However, these faster TIA-based photodetectors (pixels) tend use larger and more powerful amplifiers to increase the gain at higher frequencies. Due to the larger size and greater power requirements of TIA-based pixels, TIA-based image sensors tend to have fewer pixels than CMOS APS image sensors, sacrificing image resolution for speed.

To increase the rate at which CMOS APS image sensors can sample VLC signals while preserving the ability to scale to higher image resolutions, the token-based pixel selection (TBPS) architecture was introduced [9]; by reading only the pixels that receive VLC signals, TBPS CMOS APS image sensors can scan images much faster than traditional (windowing) CMOS APS image sensors can, thus, enabling TBPS image sensors to capture high-bandwidth VLC signals.

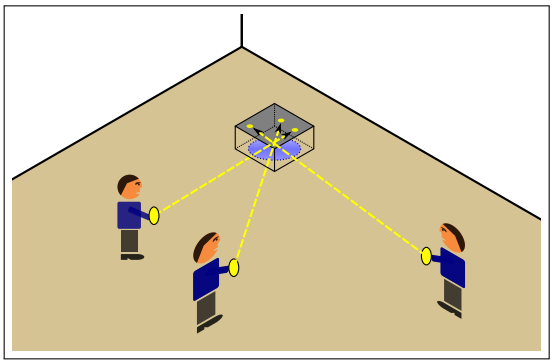

Fig. 1. Multiple users simultaneously transmit data to an imaging VLC receiver. Since each user's signal lands on a separate set of pixels, all transmissions are received without interference between users.

This ability to quickly sample many pixels enables a variety of additional applications. When the imaging VLC receiver is in focus, optical signals from spatially separate transmitters land on different pixels with very little overlap between signals. As a result, TBPS CMOS APS imaging receivers can simultaneously receive high data-rate signals from multiple transmitters with very little interference between transmitters.

This capability is especially useful in multi-user use cases, for which the VLC receiver can support additional users without degrading the performance of each user. For example, as illustrated in Fig. 1, a cellular base station or indoor VLC access point could provide a spatially-separate uplink channel for each user, allowing all of them to simultaneously use the same bandwidth without contention. Similarly, in vehicle-to-vehicle communications, this capability can help ensure that safety-critical messages are not delayed or lost due to contention or interference.

Another potential use of TBPS CMOS APS is spatial multiplexing: since the imaging VLC receiver can simultaneously receive from multiple transmitters without reducing the data rate from each transmitter, the received data rate can be increased by dividing the data stream so that each transmitter simultaneously transmits a different portion of the data. This

TABLE I
SUMMARY OF SYMBOLS

A	Gain constant
B	Signal bandwidth
C	Capacitance at node A
f_0	Nominal oscillator frequency
Δf	Half-power oscillator bandwidth
g_a	Voltage gain from node A to node B
g_b	Voltage gain of the output amplifier
$h(t)$	Impulse response of the pixel
$H(...)$	Frequency response of the pixel
$\Delta H(...)$	Incremental change in the frequency response
$I_A(t)$	Photodiode current into node A
j	$\sqrt{-1}$
$P_{opt}(t)$	Received optical power as a function of time
q	Oscillator Q factor
$Q(\cdot)$	Complementary Gaussian cumulative distribution function
R	Photodiode responsivity
t_0	Sampling cycle start time
T_{cycle}	Sampling period
T_{int}	Exposure time
T_{rst}	Duration of reset time
ΔT_{int}	Incremental change in exposure time
$u(t)$	Unit step function
ΔV_{out}	Output sample value of the CMOS active pixel
$\Delta V_{out}[i]$	The i-th output sample of the CMOS active pixel
$x(t)$	Input signal of the LSI model
$y(t)$	Output signal of the LSI model
$y[i]$	The i-th output sample of the LSI model
η	Relative error of the sample due to clock jitter
σ	Standard deviation of the exposure time due to clock jitter
τ_0	Nominal oscillator period
$\Delta\tau$	Half-power range of oscillator periods
$\Delta\tau_{int}$	Half-power range of the exposure time due to clock jitter
ω	Angular frequency ($\omega = 2\pi f$)

technique can be applied to indoor VLC systems where each luminaire provides both illumination and VLC; in these dual-use VLC systems, lighting-quality and energy-efficiency requirements may limit the data rate of each VLC transmitter; fortunately, many indoor spaces use multiple luminaires (and hence, multiple VLC transmitters) for lighting, which provides opportunities to increase downlink data rates through spatial multiplexing.

To better understand CMOS active pixel sensors in their role as VLC receivers, we model the CMOS APS pixel as a linear shift-invariant (LSI) system. Through this LSI model, we derive the frequency response of the pixel, determine the optimal exposure time for each sample (considering the trade-offs between gain and bandwidth), and investigate the pixel's sensitivity to clock jitter.

In Section II, this paper explains the operation of a CMOS active pixel; the corresponding LSI model is presented in Section III. Using this model, Section IV determines the frequency response of the CMOS active pixel. Section V, investigates the effects of varying the exposure (i.e., integration) time on the frequency response. Within this section, Subsection V-A determines the optimal duration for the exposure time of a CMOS active pixel and Subsection V-B presents bounds on the noise caused by variations in exposure time. Finally, Section VI reviews the main contributions presented in this paper and concludes the paper.

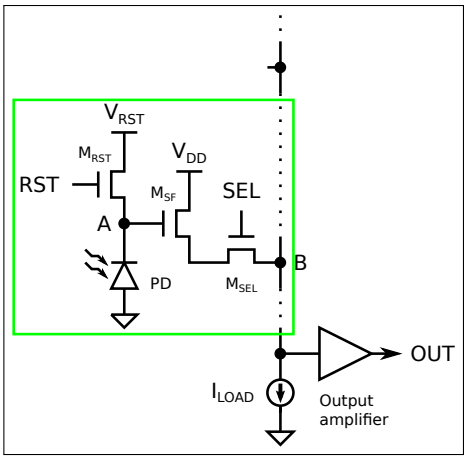

Fig. 2. A three transistor (3T) CMOS active pixel is shown in the green box. Parts, signals, and nodes are labeled. Several pixels may share the same output.

II. CMOS ACTIVE PIXELS

A basic three-transistor CMOS active pixel, connected to a shared column read-out, is shown in Fig. 2. Although many variations exist, their basic operation is the same.

Before a new measurement is taken, at time t_0, the charges stored at node A of the pixel is reset to erase the effects of all previous measurements on the new measurement. Due to the parasitic capacitance at node A and the resistance of the reset transistor, $\mathsf{M_{RST}}$, reset requires a duration of T_{rst} time.

After the pixel is reset, starting at time $t_0 + T_{rst}$, photons incident on the photodiode create electron-hole pairs that allow current to flow from node A to ground. Using a small-signal model,[1]

$$I_A(t) = -RP_{opt}(t) \tag{1}$$

where I_A is the current flowing into node A through the photodiode, R is the photodiode's responsivity to the incoming light, and P_{opt} is the captured radiant flux.

After, an exposure time of T_{int}, at time $t_0 + T_{rst} + T_{int}$, the accumulated charge, which represents the total number of photons detected during the exposure time, is amplified as a change in voltage and sampled by an analog-to-digital converter (ADC).

From Equation 1, since

$$I_A(t) = C\frac{dV_A(t)}{dt} \tag{2}$$

where C and V_A are the parasitic capacitance and voltage at node A respectively, at time $t_0 + T_{rst} + T_{int}$,

$$\Delta V_A = -\frac{R}{C}\int_{t_0+T_{rst}}^{t_0+T_{rst}+T_{int}} P_{opt}(t)dt \tag{3}$$

[1]Very large optical signals can overexpose the pixel and cause signal clipping: a non-linear distortion. Large input signals can also cause non-linear distortions by effectively changing the parasitics and gains of the electronic components within each pixel. Small-signal models assume that the input signals are small enough to avoid such non-linear distortions, which are common to most active electronic amplifiers. Practically, the effects of these distortions due to large input signals can be mitigated by adjusting the exposure time and through careful electronic design.

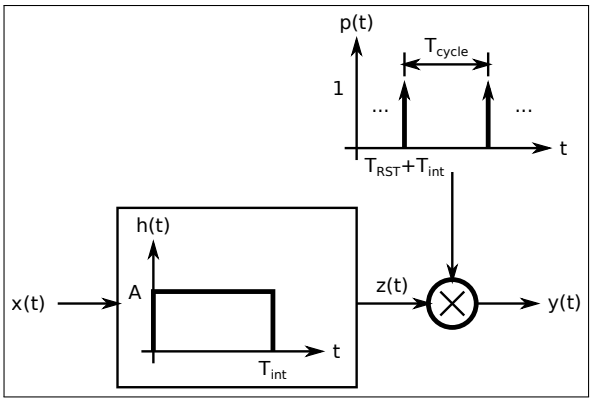

Fig. 3. The linear shift-invariant model of a CMOS active pixel is presented with input $x(t)$, impulse response $h(t)$, sampling pulse train $p(t)$, and output $y(t)$.

ΔV_A, the change in voltage at node A across the exposure time, is transferred to node B by source-follower $\mathsf{M_{SF}}$ when transistor $\mathsf{M_{SEL}}$ turns on. Node B is then amplified, sampled, and read-out.

Using a small-signal model for the source-follower $\mathsf{M_{SF}}$ and transistor $\mathsf{M_{SEL}}$,

$$\Delta V_B = g_a \Delta V_A \tag{4}$$

where g_a is the small-signal voltage gain from node A to node B, and ΔV_B is the corresponding change in voltage at node B.

Assuming that the output amplifier is linear,

$$\Delta V_{OUT} = g_b \Delta V_B = g_b g_a \Delta V_A \tag{5}$$

where ΔV_{OUT} is the change in output voltage at OUT during the exposure time and g_b is the small-signal gain of the output amplifier.

For simplicity, we assume that ΔV_{OUT}, instead of V_{OUT}, is measured by the ADC. Measuring the latter would simply add a DC offset equal to the starting (reset) value of V_{OUT}.

III. Linear Shift-Invariant Model

We propose the linear shift-invariant (LSI) model illustrated in Fig. 3 for the CMOS active pixel. In this model, the input signal, $x(t)$, is the received optical signal; given that LED-based VLC systems use intensity modulation, the received optical signal is the captured radiant flux:

$$x(t) = P_{opt}(t) \tag{6}$$

This input signal is convolved against impulse response function $h(t)$ of the CMOS active pixel. The resulting signal $z(t)$ is then sampled via multiplication against pulse train $p(t)$ to yield output $y(t)$.

As the plot of $p(t)$ shows in Fig. 3, we assume that the pixel is periodically sampled with period T_{cycle}. For notational convenience, we define time $t = 0$ so that the i-th reset-expose-readout cycle for a pixel starts at time $t = iT_{cycle}$; as a result, the i-th sample, $y[i]$, is taken at time $t = iT_{cycle} + T_{rst} + T_{int}$.

We demonstrate the validity of this LSI model by showing for each reset-expose-readout cycle, that given the same input signal, both the LSI model and the CMOS active pixel output the same samples.

As explained in Section II, ΔV_{OUT} is the output sample for one reset-expose-readout cycle of the CMOS active pixel. Plugging Equation 3 into Equation 5 and applying Equation 6, the sample readout for the i-th reset-expose-readout cycle of the CMOS active pixel is

$$\Delta V_{OUT}[i] = -g_b g_a \frac{R}{C} \int_{t_0+T_{rst}}^{t_0+T_{rst}+T_{int}} x(t)dt \tag{7}$$

where $t_0 = iT_{cycle}$ and $\Delta V_{OUT}[i]$ is the value of ΔV_{OUT} for the i-th sample.

For the LSI model,

$$z(t) = x(t) * h(t) = A \int_{t-T_{int}}^{t} x(\tau)d\tau \tag{8}$$

where $*$ denotes convolution.

Sampling $z(t)$ using impulse train $p(t)$ yields impulse train $y(t)$, in which the amplitude of each impulse is a sampled value. In discrete time, the i-th sample produced by this LSI system is

$$y[i] = A \int_{iT_{cycle}+T_{rst}}^{iT_{cycle}+T_{rst}+T_{int}} x(\tau)d\tau \tag{9}$$

where $y[i]$ is the value of $z(t)$ at time $t = iT_{cycle} + T_{rst} + T_{int}$.

Since t_0 for the i-th cycle equals iT_{cycle}, Equations 7 and 9 show that, given the same input signal, the LSI model produces the same output samples as the CMOS active pixel (i.e., $y[i] = \Delta V_{OUT}[i]\ \forall i = \{0, 1, 2, ...\}$) when

$$A = -\frac{g_b g_a R}{C} \tag{10}$$

Hence, the LSI model accurately represents the transfer function of the CMOS active pixel as described.

Note that like with continuous-time signals in linear time-invariant (LTI) systems, different frequencies in discrete time signals remain orthogonal in LSI systems. As a result, this LSI property enables CMOS APS pixels to support advanced modulation schemes like ACO- and DCO-OFDM (described in [10]), which require linearity to prevent inter-carrier interference (ICI).

IV. Frequency Response of the CMOS Active Pixel

The LSI model shows that when the sampling rate is sufficient to avoid aliasing, the frequency response of the CMOS active pixel is primarily determined by the modeled impulse response,

$$h(t) = A\left(u(t) - u(t - T_{int})\right) \tag{11}$$

where $u(t)$ is the unit step function.

Applying the Fourier transform, we get the frequency response,

$$H(\omega) = Ae^{-j\omega T_{int}/2} \cdot \frac{2\sin(\omega T_{int}/2)}{\omega} \tag{12}$$

where $j \triangleq \sqrt{-1}$ and ω is the angular frequency ($\omega = 2\pi f$ where f is the frequency). As before, the constant factor A

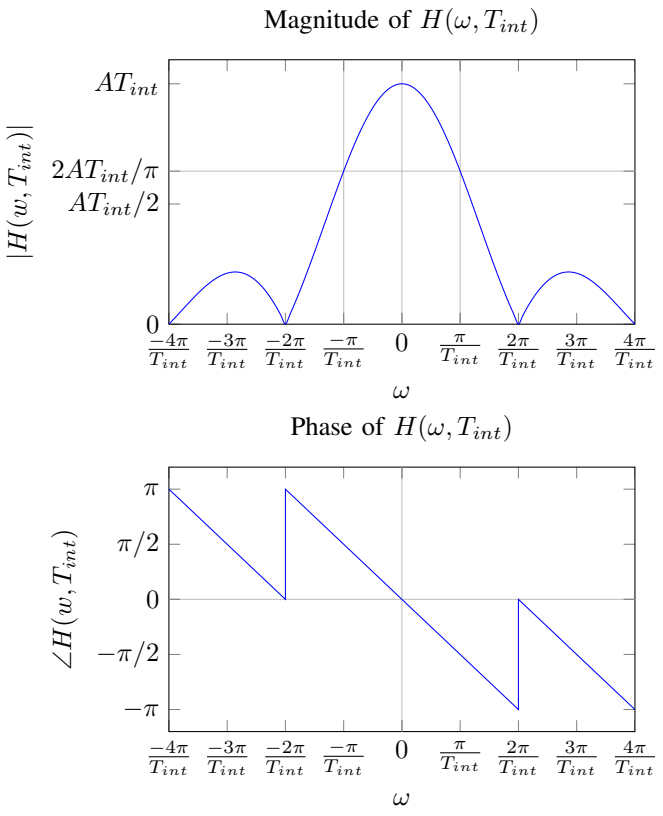

Fig. 4. The frequency response $H(w, T_{int})$ of CMOS active pixels is plotted as magnitude and phase. Phase is specified as radians.

represents the responsivity of the photodiode and the electrical amplification provided by the pixel's electronics.

The sinc factor $2\sin(\omega T_{int}/2)/\omega$ represents the frequency response of integrating the input signal over the exposure time. As shown in the magnitude plot of the frequency response in Fig. 4, this integration over time behaves as a low-pass filter: the CMOS active pixel has the highest gain of AT_{int} at $\omega = 0$ and the gain drops to 0 as ω increases to $2\pi/T_{int}$.

The complex exponential factor $e^{-j\omega T_{int}/2}$ represents the delay of $T_{int}/2$ time between the center of the exposure and when the sample is actually read. This is shown in Fig. 4 as a gradual decrease in phase with respect to w. The jumps in phase seen at $\omega = \pm 2\pi/T_{int}$ are due to transitions between positive and negative values of $H(\omega)$.

V. Variations in Exposure Time

The magnitude plot of the frequency response in Fig. 4 shows that the DC gain is proportional to the exposure time, T_{int}, and that the low-pass cutoff frequency decreases with increasing exposure time. Since the frequency response of the CMOS active pixel varies with changes in the exposure time, random variations in the duration of the exposure time may cause random errors in the samples read out by the pixel. These random variations in T_{int} may be caused by clock-jitter in the receiver's clock. To characterize this clock-jitter-induced noise, we investigate how small changes in T_{int} affect

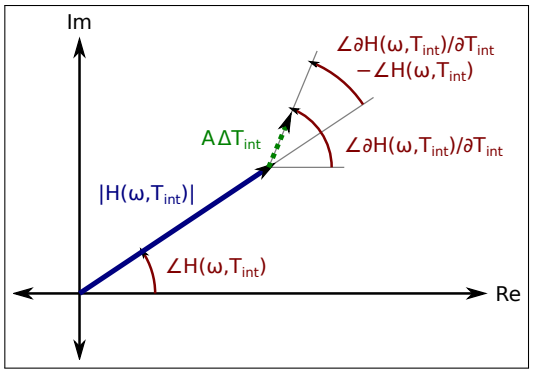

Fig. 5. These vectors on the complex plane illustrate how changes in T_{int} affect the frequency response of the CMOS active pixel. $|H(\omega, T_{int})|$ and $\angle H(\omega, T_{int})$ are plotted in Fig. 4. The magnitude $A\Delta T_{int}$ is constant with respect to ω and T_{int}. The relative phase $\angle\partial H(\omega, T_{int})/\partial T_{int} - \angle H(\omega, T_{int})$ is plotted in Fig. 6.

the frequency response of the CMOS active pixel.

For a small change of ΔT_{int} in the exposure time, the incremental change in the frequency response can be approximated as

$$\Delta H(\omega, T_{int}, \Delta T_{int}) \approx \Delta T_{int} \frac{\partial H(\omega, T_{int})}{\partial T_{int}} \tag{13}$$

Taking the partial derivative of $H(\omega, T_{int})$ with respect to the exposure time,

$$\frac{\partial H(\omega, T_{int})}{\partial T_{int}} = Ae^{-j\omega T_{int}} \tag{14}$$

Plugging Equation 14 into Equation 13, yields

$$\Delta H(\omega, T_{int}, \Delta T_{int}) \approx A\Delta T_{int} e^{-j\omega T_{int}} \tag{15}$$

Fig. 5 illustrates this incremental change to the pixel's frequency response as the summation of two vectors on the complex plane: $H(\omega, T_{int}) + \Delta H(\omega, T_{int}, \Delta T_{int})$. $\Delta H(\omega, T_{int}, \Delta T_{int})$, represented by the green (dotted-line) vector, has a constant magnitude and a phase that changes with frequency.

For any ω, when the phases of $\Delta H(\omega, T_{int}, \Delta T_{int})$ and $H(\omega, T_{int})$ are within $\pi/2$ radians of each other, the two vectors add constructively, increasing the gain of the frequency response at this angular frequency. Otherwise, $H(\omega, T_{int})$ and $\Delta H(\omega, T_{int}, \Delta T_{int})$ add destructively, decreasing the gain of the frequency response at that frequency.

This difference in phase is plotted in Fig. 6 for a positive ΔT_{int}; (a negative ΔT_{int} would shift the phase difference at all frequencies by π radians). As shown, for angular frequencies $|\omega| < \pi/T_{int}$, $H(\omega, T_{int})$ and $\partial H(\omega, T_{int})/\partial T_{int}$ are always in phase. This means that for all ω in the range $|\omega| < \pi/T_{int}$, longer exposure times yield a more gain.

A. Optimal Duration for Exposure Time

Building on this analysis of the effects of variations in exposure time on the frequency response of the CMOS active pixel, we show that although longer exposure times attenuate higher-frequency signals, the optimal exposure time (to maximize

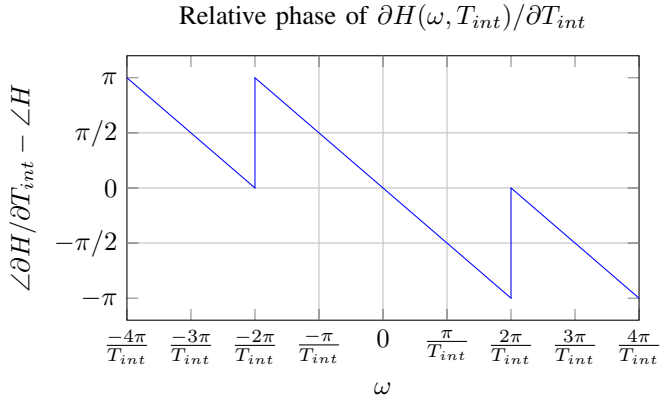

Fig. 6. $\partial H(\omega, T_{int})/\partial T_{int}$ adds constructively with frequency response $H(\omega, T_{int})$ when the difference in phase (i.e., the ordinate) is between $-\pi/2$ and $\pi/2$ radians; otherwise, they add destructively.

the gain or sensitivity of the pixel across all received signal frequencies) is as long as possible.

Assuming that the pixel is sampled at at least the Nyquist rate, we show that the input signal must be band-limited so that all signal power is contained within the band $|\omega| < \pi/T_{int}$. Given that the duration of the exposure time, T_{int}, must fit within the sampling period, T_{cycle},

$$T_{int} \leq T_{cycle} \tag{16}$$

Therefore (for non-zero exposure times and sampling periods),

$$\frac{\pi}{T_{int}} \geq \frac{\pi}{T_{cycle}} \tag{17}$$

Applying the Nyquist criterion, the sampling rate $1/T_{cycle}$ is greater than twice the bandwidth B of the input signal:

$$2\pi B < \frac{\pi}{T_{cycle}} \tag{18}$$

Combining the definition of signal bandwidth with Equations 17 and 18, all signal power must be contained within

$$|\omega| \leq 2\pi B < \frac{\pi}{T_{cycle}} \leq \frac{\pi}{T_{int}} \tag{19}$$

As explained earlier in Section V, increasing the exposure time by a positive ΔT_{int} increases the gain of the frequency response for all frequencies $|\omega| < \pi/T_{int}$. Since all input signals (assuming that the Nyquist criterion is satisfied) are within this range of frequencies, increasing the exposure time will always increase the signal gain across the entire bandwidth of the input signal, and hence, increase the channel capacity.

Although in many other cases, increasing the integration time would sacrifice bandwidth for gain, in this case, the Nyquist criterion (to avoid aliasing) places a tighter bound on the available bandwidth than the frequency response of the longest possible exposure time. As a result, higher-frequency signals that would have been attenuated would not have been used anyway.

For any given sampling period, the longest possible exposure time is optimal. To achieve this optimal exposure time, the CMOS active pixel should be reset immediately after its previous sample is read out.

B. Bounding the Noise Caused by Clock-Jitter

The stability of clocks are often characterized by their oscillator's Q factor, q:

$$q = f_0/\Delta f \tag{20}$$

where f_0 is the nominal frequency of the clock and Δf is the half-power bandwidth [11, p. 91].

Computing the corresponding half-power range of periods for the oscillator,

$$\Delta\tau = \frac{1}{f_0 - \Delta f/2} - \frac{1}{f_0 + \Delta f/2} = \frac{1}{f_0(q - \frac{1}{4q})} \tag{21}$$

For large q values,

$$\Delta\tau \approx \frac{1}{f_0 q} = \frac{\tau_0}{q} \tag{22}$$

where τ_0 is the nominal period of the oscillator.

Given that the exposure time, T_{int}, is some constant times the oscillator's period, τ_0, the half-power range of exposure times is

$$\Delta\tau_{int} \approx \frac{T_{int}}{q} \tag{23}$$

Using $\Delta\tau_{int}$ as the full width at half maximum (FWHM) and assuming that the clock jitter has a Gaussian distribution, ΔT_{int} is a Gaussian random variable with a mean of 0 and a standard deviation of

$$\sigma = \frac{\Delta\tau_{int}}{2\sqrt{2\ln 2}} \approx \frac{1}{2\sqrt{2\ln 2}} \frac{T_{int}}{q} \tag{24}$$

Defining the relative error η as the ratio of the absolute error to the magnitude of the correct value, where the absolute error is the difference between the correct value and the sampled value, we note that the relative error of the sample is the same as the relative error of the gain of the frequency response.

$$\eta = \frac{|H(\omega, T_{int} + \Delta T_{int}) - H(\omega, T_{int})|}{|H(\omega, T_{int})|} \tag{25}$$

From the linear approximation illustrated in Fig. 5, the numerator of η is approximately $|A\Delta T_{int}|$. Given the bound for ω in Equation 19, the denominator of η is at least $|2AT_{int}/\pi|$, as shown in Fig. 4. Using this numerator and this lower bound on the denominator, η can be approximately bounded as

$$\eta \leq \left| \frac{A\Delta T_{int}}{2AT_{int}/\pi} \right| = \frac{\pi\,|\Delta T_{int}|}{2T_{int}} \tag{26}$$

Since ΔT_{int} is a Gaussian random variable (with the standard deviation described in Equation 24),

$$\begin{aligned} \Pr[\eta > \eta_{max}] \leq\ & \Pr\left[\frac{\pi|\Delta T_{int}|}{2T_{int}} > \eta_{max}\right] = \\ & 2\Pr\left[\Delta T_{int} > \frac{2\eta_{max} T_{int}}{\pi}\right] \end{aligned} \tag{27}$$

$$\Pr[\eta > \eta_{max}] \leq 2Q\left(\frac{4\sqrt{2\ln 2} \cdot q\eta_{max}}{\pi}\right) \tag{28}$$

where $Q(z)$ is the complementary Gaussian cumulative distribution function; that is $Q(z)$ is the probability that a standard normal random variable Z is greater than z.

For crystal oscillators, with typical Q factors of $10^4 \leq q \leq 10^6$ [11, p. 633], the relative error η for the sample can be bounded fairly tightly with great certainty. For example, using $q = 10^4$,

$$\Pr[\eta > 5 \times 10^{-4}] \leq 2Q(7.49) = 6.9 \times 10^{-14}$$

This bound guarantees with very high certainty for $q \geq 10^4$ that the noise due to variations in exposure time caused by clock jitter is negligible: except with negligible probability, the relative error of the sample due to clock jitter on the exposure time is several orders of magnitude smaller (-66 dB) than the correct value.

In contrast, for a lower q, such as for $q = 10$ for an on-chip oscillator, the error due to variations in integration time can be much more significant. For this reason, we recommend using a stable clock source in reset-integrate-and-sample receivers.

VI. Conclusion

Research into visible light communications is often divided into two domains: one for low-cost applications (which typically use readily available CMOS APS cameras found in smart phones and other consumer devices) and another for high data-rate applications (which typically use specialized high-bandwidth TIA-based photodetectors to maximize performance). In our previous paper, we showed that CMOS APS image sensors can also be adapted to receive high-bandwidth VLC signals with token-based pixel selection (TBPS) [9], merging the two domains of visible light communication.

To analyze the CMOS APS image sensor for high-bandwidth applications, this paper models the CMOS active pixel as a linear and shift-invariant (LSI) system. Using this LSI model, we derived the frequency response of CMOS active pixels and began to explore two design decisions for CMOS-APS-based VLC receivers: the gain-bandwidth trade-off for increasing exposure time and the clock stability required for the receiver.

Although additional developments (such as algorithms to track VLC signals as they move across an image sensor) are needed to fully realize the potential of CMOS-APS-based VLC receivers, we believe that CMOS APS image sensors are a promising alternative to TIA-based VLC receivers for high data-rate VLC. Not only can CMOS active pixels (as LSI systems) support the same advanced modulation schemes as TIA-based VLC receivers (such as OFDM), CMOS active pixel sensors can also scale to much higher resolutions than TIA-based VLC receivers. In turn, this higher resolution can yield finer electronic tracking for mobile use cases and better performance in multi-transmitter or multi-user scenarios.

In addition to improving high data-rate applications of VLC, merging the two domains also suggests ways to improve low-cost applications of VLC, such as time-varying 2D visual codes. For example, the frequency response shown in Fig. 4 shows that even at slow frame rates, visual codes are affected by the low-pass nature of the channel as the visual codes change over time. By applying techniques such as equalization or OFDM, visual codes used in low-cost VLC applications can be adapted to more efficiently use the VLC channel. In our future work, we investigate how techniques used for high data-rate applications of VLC can be applied to improve low-cost applications of VLC.

Acknowledgment

This work was supported primarily by the Engineering Research Centers Program of the National Science Foundation under NSF Cooperative Agreement No. EEC-0812056.

References

[1] A. Wang, S. Ma, C. Hu, J. Huai, C. Peng, and G. Shen, "Enhancing reliability to boost the throughput over screen-camera links," in *Proceedings of the 20th Annual International Conference on Mobile Computing and Networking*, ser. MobiCom '14. New York, NY, USA: ACM, 2014, pp. 41–52. [Online]. Available: http://doi.acm.org/10.1145/2639108.2639135

[2] W. Hu, J. Mao, Z. Huang, Y. Xue, J. She, K. Bian, and G. Shen, "Strata: Layered coding for scalable visual communication," in *Proceedings of the 20th Annual International Conference on Mobile Computing and Networking*, ser. MobiCom '14. New York, NY, USA: ACM, 2014, pp. 79–90. [Online]. Available: http://doi.acm.org/10.1145/2639108.2639132

[3] C. Danakis, M. Afgani, G. Povey, I. Underwood, and H. Haas, "Using a CMOS camera sensor for visible light communication," in *3rd IEEE Workshop on Optical Wireless Communications (OWC'12)*, Dec 2012, pp. 1244–1248.

[4] G. Woo, A. Lippman, and R. Raskar, "VRCodes: Unobtrusive and active visual codes for interaction by exploiting rolling shutter," in *Mixed and Augmented Reality (ISMAR), 2012 IEEE International Symposium on*, Nov. 2012, pp. 59 –64.

[5] S. Arai, S. Mase, T. Yamazato, T. Endo, T. Fujii, M. Tanimoto, K. Kidono, Y. Kimura, and Y. Ninomiya, "Experimental on hierarchical transmission scheme for visible light communication using LED traffic light and high-speed camera," in *Vehicular Technology Conference, 2007. VTC-2007 Fall. 2007 IEEE 66th*, Sept.–Oct. 2007, pp. 2174 – 2178.

[6] S. Okada, T. Yendo, T. Yamazato, T. Fujii, M. Tanimoto, and Y. Kimura, "On-vehicle receiver for distant visible light road-to-vehicle communication," in *Intelligent Vehicles Symposium, 2009 IEEE*, June 2009, pp. 1033 –1038.

[7] S. Nishimoto, T. Yamazato, H. Okada, T. Fujii, T. Yendo, and S. Arai, "High-speed transmission of overlay coding for road-to-vehicle visible light communication using LED array and high-speed camera," in *3rd IEEE Workshop on Optical Wireless Communications (OWC'12)*, Dec 2012, pp. 1234–1238.

[8] I. Takai, S. Ito, K. Yasutomi, K. Kagawa, M. Andoh, and S. Kawahito, "LED and CMOS image sensor based optical wireless communication system for automotive applications," *Photonics Journal, IEEE*, vol. PP, no. 99, pp. 1–1, 2013.

[9] J. C. Chau and T. D. Little, "Scalable imaging VLC receivers with token-based pixel selection for spatial multiplexing," in *Proceedings of the 1st ACM MobiCom Workshop on Visible Light Communication Systems*. ACM, September 2014, pp. 21–26.

[10] J. Armstrong, "OFDM for optical communications," *J. Lightwave Technol.*, vol. 27, no. 3, pp. 189–204, Feb 2009. [Online]. Available: http://jlt.osa.org/abstract.cfm?URI=jlt-27-3-189

[11] T. H. Lee, *The Design of CMOS Radio-Frequency Integrated Circuits*, 2nd ed. Cambridge University Press, 2006.